Auroral structure and dynamics from GOLD

R. G. Michell,[1,2]

R. G. Michell, University of Maryland, College Park, MD, USA

NASA Goddard Space Flight Center, Greenbelt, MD, USA. (robert.g.michell@nasa.gov)

[1]Department of Astronomy, University of

Maryland, College Park, MD, USA

[2]NASA Goddard Space Flight Center,

Greenbelt, MD, USA

Abstract. The Global-scale Observations of the Limb and Disk (GOLD) mission data contain significant quantitative information about the aurora on a global scale. Here we present techniques for quantifying such information, including the temporal development of the structure within the auroral oval using the GOLD images. These techniques are applied to auroral observations in the GOLD data, in particular showing an example of how the longitudinal structure within the aurora varies over the course of six consecutive days with differing levels of geomagnetic activity. A simple model of the solar-induced airglow is presented that is used to remove the sunlight contamination from the dayside auroral observations. Comparisons to ground-based auroral imaging are used for the overall auroral context and to make estimates of the proportionality between the intensities of the green-line (557.7 nm) emission in the visible and the 135.6 nm emissions in the GOLD data. These observations are consistent with the intensity of the 135.6 nm auroral emission being on the same order as the intensity of the 557.7 nm auroral emission. They were both found to be around 1 kR for a stable auroral arc on a day with low geomagnetic activity (03 November 2018) and around 10 kR for an active auroral display on a day with higher levels of geomagnetic activity (05 November 2018). This could have important implications for making direct comparisons between space-based UV auroral imaging and ground-based visible-light auroral imaging and the total energy input estimates that are derived from them.

1. Introduction

The Global-scale Observations of the Limb and Disk (GOLD) mission [*Eastes et al.*, 2017] consists of an ultraviolet (UV) spectrograph on a geostationary satellite and thus can provide global scale images of Earth that contain the UV signatures of the aurora. When observing the aurora from space, the auroral emissions that occur in the far ultraviolet (FUV) part of the spectrum have certain advantages over those in the visible wavelengths. One of the main advantages of the far ultraviolet (∼130 nm to ∼190 nm) is that the atmosphere efficiently absorbs these wavelengths and thus from a space-based vantage point, there is essentially no background of scattered light from the ground, as you would have when imaging in visible wavelengths. Thus making dayside and nightside auroral observations possible. However, this also means that these UV auroral emissions are completely unobservable from a ground-based vantage point. The atmospheric absorption of these FUV auroral emissions is also dependent on wavelength and thus (within the GOLD passband) the shorter wavelengths are more absorbed than the longer wavelengths. Therefore, it is possible to use the ratio of the intensities of the shorter wavelengths to the longer wavelengths (within the far ultraviolet band) to estimate the altitude at which the emissions are coming from and hence the characteristic (average) energy of the precipitating electrons [*Unick et al.*, 2016]. The total intensity of the aurora within these bands is considered to be proportional to the total electron flux [*Unick et al.*, 2016], however it is not as straightforward as it is with the 427.8 nm N_2^+ emissions [*Rees and Luckey*, 1974] in the visible [*Murphree*, 1998].

Quantifying the total energy influx into the aurora and the average energy of the precipitating electrons is fundamental to characterizing the aurora and its effects on the thermosphere, including ionospheric conductivity. Techniques for extracting these parameters from UV imaging of the aurora have been described in the literature [*Strickland et al.*, 1983; *Lummerzheim et al.*, 1991; *Germany et al.*, 1997]. These techniques are summarized in *Germany et al.* [1997] where they describe a technique that uses the ratio of an LBH low band (centered around 150 nm) and an LBH high band (centered around 170 nm) for inferring these fundamental auroral electron characteristics. The only significant excitation mechanism for the LBH emissions is electron impact ionization, therefore in the absence of photo-electrons, the LBH emissions act as a direct proxy for incident electron precipitation fluxes [*Germany et al.*, 1997]. The O_2 Schumann-Runge (S-R) absorption peaks within the FUV portion of the spectrum and decreases with longer wavelengths. Therefore if the incident electron energies are high enough to penetrate deep enough into the atmosphere, where there is a significant amount of O_2, there will be differential absorption as a function of wavelength. The shorter wavelengths (LBH-Low) will be absorbed more than the longer wavelengths (LBH-High) and therefore the ratio of these will vary significantly with increasing depth (decreasing altitude) hence with increasing average electron energy. Thus the ratio of the LBH-Low (with higher absorption due to O_2) to the LBH-High (with less absorption due to O_2) can be used as a proxy for the average electron energy. This ratio is calculated from 2 different emission bands from the same species and thus will be independent of any compositional changes that can occur, such as the significant changes in the O-to-N_2 ratio that can be associated with certain auroral activity. The LBH-High intensity can be used (in conjunction with simple transport mod-

eling) to estimate the incident total energy flux of electrons. Another important emission in the FUV is the 135.6 nm emission from atomic oxygen (OI).

Figure 1 shows a representation of the auroral spectrum in the FUV, showing the relative intensities of the main emission lines. The three main spectral regions of interest in the typical GOLD analyses (135.6 nm, LBH-Low and LBH-High) are denoted by the colored boxes. In Summary: the overall GOLD passband is 134 nm to 166 nm; the 135.6 nm band is the sum of the emissions between 133 nm and 137 nm; the LBH-Low band is the sum of the emissions between 140 nm and 148 nm and the LBH-High band is the sum of the emissions between 150 nm and 160 nm.

The main goal of this work is to demonstrate the usefulness of GOLD data, in particular the dayside GOLD observations, for quantifying the auroral structure and dynamics and to show that time-series of the auroral development over single days and many days can be created from these data. In addition, the nightside GOLD data can also be used to examine higher time resolution aspects of the auroral development over shorter timescales and without any solar contamination. An initial comparison is also made between the intensities of ground-based images in the visible (557.7 nm) and the space-based GOLD images in the FUV (135.6 nm).

2. Observations

The GOLD data contained in the available CDF files contain northern and southern hemisphere disk images across the whole GOLD passband and thus they can be summed into different wavelength bands of interest. The disk images of radiance are summed together into the appropriate wavelength bands (listed above and shown in Figure 1) in order to reproduce the disk images, such as those provided in the Level 1D summary plots,

where the aurora can clearly be identified. As a demonstration of the utility of the GOLD data for auroral observation, six consecutive days in early November 2018 were chosen for initial analysis. This time period was chosen because ground-based auroral observations taken from Poker Flat, AK were used to identify different levels of auroral activity and there were six days in a row (01 – 06 November 2018) that had clear visibility from Poker Flat, AK with varying levels of auroral activity. Initially, two days were examined, one day that had minimal auroral activity (03 November 2018) and another day (05 November 2018) that had strong auroral activity. Figure 2 shows GOLD disk images (in 135.6 nm) of the northern hemisphere for these two separate nights in November 2018. These were taken in the dawn-sector and at the same local time each night (07:16 UT). The 135.6 nm emission band was chosen for display because it has the brightest signal of the 3 main bands (as discussed above in Figure 1).

Figure 3 shows keograms that were constructed from the ground-based all-sky camera data (taken in the 557.7 nm band) by extracting a north-south intensity cut through an image every 5-seconds then subsequently stacking those lines into a 2-D array, with elevation angle of the field-of-view on the y-axis (corresponding to latitude) and time on the x-axis. This presentation allows for easily identifying the level of auroral activity and the latitude of the aurora throughout a given night. The black vertical line on Figure 3 shows the time at which the two GOLD images were taken (07:15 UT) on both nights.

The aurora is clearly discernible in the GOLD images, even on the quiet auroral day, thus it is likely that the aurora will be visible in some form on nearly every day and night in the GOLD dataset. Therefore the GOLD auroral data can be used to study long-term seasonal and yearly variations in the auroral activity. The global view of GOLD

allows the longitudinal structuring to be quantified. In addition, the dayside GOLD data actually contain a time series of 32 disk images of each hemisphere, with an image every half hour, covering a time period of about 15.5 hours. These series begin in the dawn-sector, continuing through the noon-sector and into the dusk-sector. Therefore it is possible to quantify the temporal development of the longitudinal structuring. As a means to quantify the amount of longitudinal structuring and its temporal development, a type of keogram is constructed by taking an intensity slice through the auroral oval in the east-west direction (actually adding together several latitudinal rows of pixels inside the auroral oval) and subsequently stacking those into a new image. Figure 4 shows a panel of such keograms taken from the middle of the auroral oval for these two days (03 and 05 November 2018) and over the three wavelength bands (135.6 nm, LBH-Low and LBH-High). In this representation, time is on the y-axis and longitude is on the x-axis.

There are several things to note from Figure 4. First, there are clear differences in auroral intensity and structuring between the day with more auroral activity (05 Nov) and the day with less auroral activity (03 Nov). Second, there are no significant differences in the structuring between the three wavelength bands, only differences in the intensity of the aurora. They are all plotted with the same intensity scale. Lastly, there is a clear contamination from the solar illumination (the diagonal bands through the middle of the keograms), when the aurora is in the daylight.

The nightside GOLD data do not suffer from solar contamination in the same way, however there are, in general, fewer images. Figure 5 shows the time series of aurora in nightside GOLD images (in the 135.6 nm band) from these two nights (03 and 05 November 2018). These images are spaced 15 minutes apart, covering 45 minutes with

the four images. These represent all of the nightside images from these two days and it is clear that global longitudinal variations are seen, even on these relatively short timescales. During the time of the dayside observations, 03 November had less auroral activity, by the night of 03 November turning into 04 November, the aurora had started to increase and was actually brighter than it was on 05 November at the same local time, however the aurora on 05 November still has a larger latitudinal extent. The GOLD nightside observations can be used to track the development of auroral features on shorter timescales (one-hour) and with an increased temporal resolution (15 minutes).

3. Discussion

The solar contamination present in the dayside GOLD auroral images presents a problem when examining the dayside aurora, especially in the noon-sector. Figure 4 clearly shows that solar induced background is present in all wavelength bands and that it is time dependent. These bands of solar-induced airglow are often brighter than the auroral structures present at high latitudes. There is essentially no solar interference in the dawn-sector, before the terminator arrives and the dusk-sector, after the terminator passes, but the middle sunlit section is clearly contaminated by solar-induced airglow. Therefore in order to quantify the sunlit auroral structures, this time-dependent background signal needs to be removed. Luckily this signal is predictable and depends highly on the solar zenith angle (which is also included in the Geo-referenced GOLD data files). In an initial attempt to remove this signal, a simple model of this solar induced background was created that is proportional to the cosine of the solar zenith angle. Figure 6 (top) shows a portion of a disk image with the auroral region of interest highlighted by a white box. Keograms are constructed by taking an intensity slice through the middle of the box and stacking

them together to create the keogram. Figure 6 (bottom) shows a comparison between a keogram created from the raw intensity (left) and one created from the intensity with the solar contamination removed by subtracting off the simple model of the solar induced background (right). In this figure, the keograms are oriented so that time is on the x-axis and longitude is on the y-axis. The case with less active aurora (03 November 2018) was chosen because this would have a weaker auroral signal and if this can be extracted, then the brighter auroral signal on more active days would be clearly visible and quantifiable.

From Figure 6 it is clear that even such a simple model of the solar induced background removes most of the contamination, which reveals much more of the sunlit auroral features, including local time and longitudinal variations within the sunlit aurora. There is still some solar contamination, especially near the terminators, because the simple model used stopped at a solar zenith angle of 90 degrees, but in reality the solar induced airglow extends beyond that due to the finite thickness of the atmosphere. Future work will include a slightly more complicated model of the dayside airglow, as discussed in *Lummerzheim et al.* [1997]. In addition, it is possible that some of the dawn-dusk asymmetry in the keograms could be a result of the simplified method currently being used to create the keograms. Currently, a few horizontal rows of pixels are averaged together (the same pixels in each image) and these are then used to create the keogram. However, it is clear from the example disk image shown in the top of Figure 6 that the auroral oval is often tilted and thus a strictly horizontal cut will miss some of the aurora on either the dawn or the dusk side depending on which pixels are used to make the cut. For the data presented here, three rows of pixels are averaged together and they were chosen to be near the center of the auroral activity. This was done in order to minimize the amount of background

signal getting into the keograms. The same pixels were used for all the nights examined. In future analysis, a more clever approach will be used for creating the keograms, where a pixel mask will be used in order to just sample the pixels where the aurora occur. The auroral pixels will be determined by examining a larger number of auroral events, especially the more active events (which can be found using the ground-based auroral imaging data) so that the maximum extent of the aurora can be determined.

The continuous coverage of the dayside aurora provided by GOLD can be used to create long time-series of these longitudinal keograms (as presented in Figure 6). Applying the simple solar background removal algorithm to six consecutive days of GOLD data reveals that the structure and dynamics within the aurora can be captured and quantified. Figure 7 shows these six keograms (in two rows) on a continuous timescale from the 135.6 nm band. These data cover 01–06 November 2018 and contain both quiet and active auroral conditions as well as the transitions between them.

This technique can be used to create a long time-series of the aurora, essentially over the life of the mission. There are gaps during the nightside in this representation, but using the available nightside data, some information could be added in. Even with just the dayside data, features of the overall auroral structure and dynamics can be quantified. For example, the aurora became active around the noon-sector on 04 November and stayed fairly active through 05 November, where the aurora became significantly brighter than the residual solar interference at the terminators, getting to a maximum brightness of around 15 kR on 04 November. On both of these active nights, the aurora showed a propagation from east to west starting in the noon-sector.

Figure 5 showed the GOLD nightside auroral images where 03 November 2018 (the quiet auroral day) showed brighter aurora than 05 November (the active auroral day). This long time-series keogram shows that the aurora at the end of 03 November (dusk) was beginning to intensify and was still intense on the beginning (dawn) of 04 November, while the aurora on the dusk side of 05 November was becoming less intense and was even less intense on the dawn-side of 06 November, which is consistent with the nightside images in Figure 5. This representation can be used to illustrate the overall behavior of certain aspects of the auroral oval over long periods of time.

The intensity of the aurora from the ground-based auroral imaging taken from Poker Flat, AK can be used to make general comparisons to the intensity of the aurora in the GOLD observations. The location of the aurora over Poker Flat, AK would however correspond to the extreme western side of the aurora visible in the GOLD images (near the limb). Thus it is not possible to make clear one-to-one comparisons of the auroral structures simultaneously visible in both data sets. However given that the overall structure of the aurora is generally longitudinally extended, especially when features persist for several hours in either data set, it is likely that both GOLD and the ground-based imagers would observe similar features. Therefore a general comparison is made between the GOLD observations shown in Figure 2 and the ground-based auroral imaging shown in Figure 3. For 05 November 2018 (the active day), the intensity of the 135.6 nm emission is observed to be around 10 kR in the GOLD data at the extreme western edge of the auroral oval (closest to AK). At the same exact time, the ground-based auroral imaging observed the average intensity of the 557.7 nm emission to also be around 10 kR. Another point of comparison and perhaps a cleaner comparison can be made for the observations

on 03 November 2018 (the quiet day) because the aurora did not change much over many hours. Here the intensity of the 135.6 nm emission in the GOLD data on the extreme western edge of the auroral oval is around 1 kR. At the same time, the ground-based imaging (Figure 3) showed a quiet auroral arc in the north that lasted for more than 6 hours and had an intensity of around 1 kR. These synergistic comparisons show that the intensities of the 135.6 nm emission and the 557.7 nm emission are on the same order. More quantitative comparisons can be made, using more days, in order to improve our estimate of the proportionality between these two emissions. Both the 135.6 nm emission and the 557.7 nm emission are from oxygen (OI) and thus it is possible that there is a clear proportionality between their intensities. This would be an important proportionality to understand because it would allow for better comparisons between ground-based and space-based auroral observations and could lead to improved estimates of auroral energy input on global scales.

4. Conclusions

The GOLD disk images contain valuable information about the structure and dynamics of the aurora. The nightside GOLD data contain short time-series that can be used to examine shorter timescale variations within the auroral oval, while the dayside observations can be used to create long time-series of auroral images and longitudinal keograms. Such keograms enable the quantification of the structure of the auroral oval and propagation of large-scale auroral features within it, especially those associated with active aurora, including substorms and the multi-day intensifications that result from magnetic storms.

The solar-induced airglow can be mostly removed from the sunlit auroral observations in the dayside GOLD data using a simple method. This method estimates the solar-

induced airglow intensity as being proportional to the cosine of the solar zenith angle and then subtracts this modeled background from the observed intensities. This works well to remove the majority of the solar contamination, but some interference remains near the terminators, due to the simplicity of the background model and the three-dimensional nature of the atmosphere. Even with such a simple model of the background, the sunlit auroral intensities can be observed above the background levels, even for moderate and weak auroral activity levels.

A synergistic comparison is made between the 135.6 nm band auroral intensity from the GOLD observation and the 557.7 nm auroral intensity observed from ground-based auroral imaging taken at Poker Flat, AK. Even though Poker Flat is not exactly within the field of view of the GOLD imager, the aurora at the extreme western edge of the auroral oval observed in the GOLD data would be fairly close to being over Alaska (within an hour of local time). Therefore, a comparison is made for the two nights examined in detail (03 and 05 November 2018) and similar intensities were observed in the 135.6 nm GOLD observations and the 557.7 nm ground-based observations. On 05 November (the more active day), the Gold observations showed the 135.6 nm aurora to be around 10 kR and the 557.7 nm aurora from the ground-based imaging was also observed to be around 10 kR. On 03 November 2018 (the less active day), the 135.6 nm band was observed to be around 1 kR and the 557.7 nm band was also observed to be around 1 kR. This 1 kR aurora in the 557.7 nm ground-based imaging data was stable and lasted for over 5 hours centered around the time of the GOLD image. Therefore the ground-based imaging and GOLD would have measured the same auroral structure, making this an accurate comparison. These observations are consistent with the intensity of the 135.6 nm auroral

emission being on the same order as the intensity of the 557.7 nm auroral emission. This could have important implications for making direct comparisons between space-based UV auroral imaging and ground-based visible-light auroral imaging and the total energy input estimates that are derived from such observations.

Acknowledgments. This work was supported in part by National Science Foundation Grant AGS1523097. The GOLD data were provided courtesy of NASA/GOLD and the mission science team and are all freely available to the public at: https://gold.cs.ucf.edu/data/.

References

Eastes, R. W., W. E. McClintock, A. G. Burns, D. N. Anderson, L. Andersson, M. Codrescu, J. T. Correira, R. E. Daniell, S. L. England, J. S. Evans, J. Harvey, A. Krywonos, J. D. Lumpe, A. D. Richmond, D. W. Rusch, O. Siegmund, S. C. Solomon, D. J. Strickland, T. N. Woods, A. Aksnes, S. A. Budzien, K. F. Dymond, F. G. Eparvier, C. R. Martinis, and J. Oberheide (2017), The Global-Scale Observations of the Limb and Disk (GOLD) Mission, *Space Sci. Rev.*, *212*(1-2), 383–408, doi:10.1007/s11214-017-0392-2.

Germany, G. A., G. K. Parks, M. Brittnacher, J. Cumnock, D. Lummerzheim, J. F. Spann, L. Chen, P. G. Richards, and F. J. Rich (1997), Remote determination of auroral energy characteristics during substorm activity, *Geophys. Res. Lett.*, *24*(8), 995–998, doi:10.1029/97GL00864.

Lummerzheim, D., M. H. Rees, J. D. Craven, and L. A. Frank (1991), Ionospheric conductances derived from DE-1 auroral images, *Journal of Atmospheric and Terrestrial Physics*, *53*, 281–292, doi:10.1016/0021-9169(91)90112-K.

Lummerzheim, D., M. Brittnacher, D. Evans, G. A. Germany, G. K. Parks, M. H. Rees, and J. F. Spann (1997), High time resolution study of the hemispheric power carried by energetic electrons into the ionosphere during the May 19/20,1996 auroral activity, *Geophys. Res. Lett.*, *24*(8), 987–990, doi:10.1029/96GL03828.

Murphree, J. (1998), Uv auroral imaging, in *Magnetospheric Research with Advanced Techniques*, *COSPAR Colloquia Series*, vol. 9, edited by R. Xu and A. Lui, pp. 51 – 59, Pergamon, doi:https://doi.org/10.1016/S0964-2749(98)80009-7.

Rees, M. H., and D. Luckey (1974), Auroral electron energy derived from ratio of spectroscopic emissions. I - Model computations, *J. Geophys. Res.*, *79*, 5181–5186, doi:10.1029/JA079i034p05181.

Strickland, D. J., J. R. Jasperse, and J. A. Whallen (1983), Dependence of auroral FUV emissions on the incident electron spectrum and neutral atmosphere, *Journal of Geophysical Research*, *88*(A10), 8051–8062, doi:10.1029/JA088iA10p08051.

Unick, C., E. Donovan, E. Spanswick, and V. Uritsky (2016), Selection of FUV auroral imagers for satellite missions, *Journal of Geophysical Research (Space Physics)*, *121*(10), 10,019–10,031, doi:10.1002/2016JA022627.

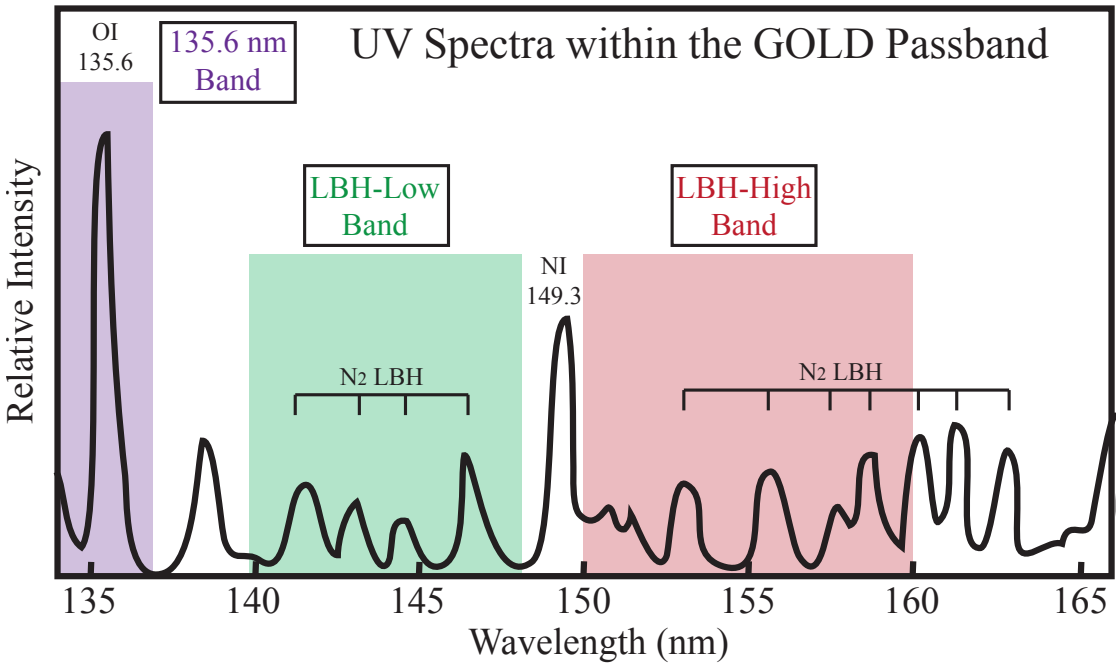

Figure 1. Representation of the FUV auroral spectra within the GOLD passband, showing the approximate relative intensities of the different auroral bands. The main spectral regions of interest that are defined in the GOLD data products guide are shown as the different colored boxes.

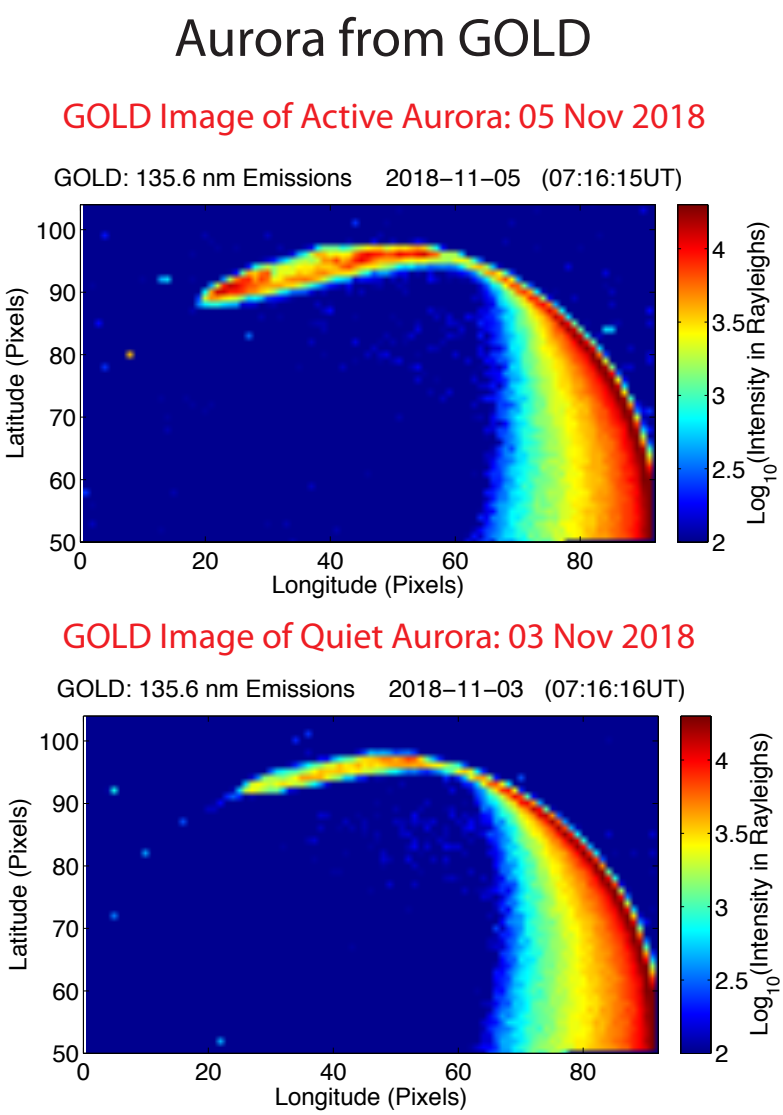

Figure 2. GOLD disk images (in the 135.6 nm band) of the northern hemisphere aurora, for an active night (05 Nov) and a quiet night (03 Nov) Both images are taken at the same local time (07:16 UT) in the dawn-sector.

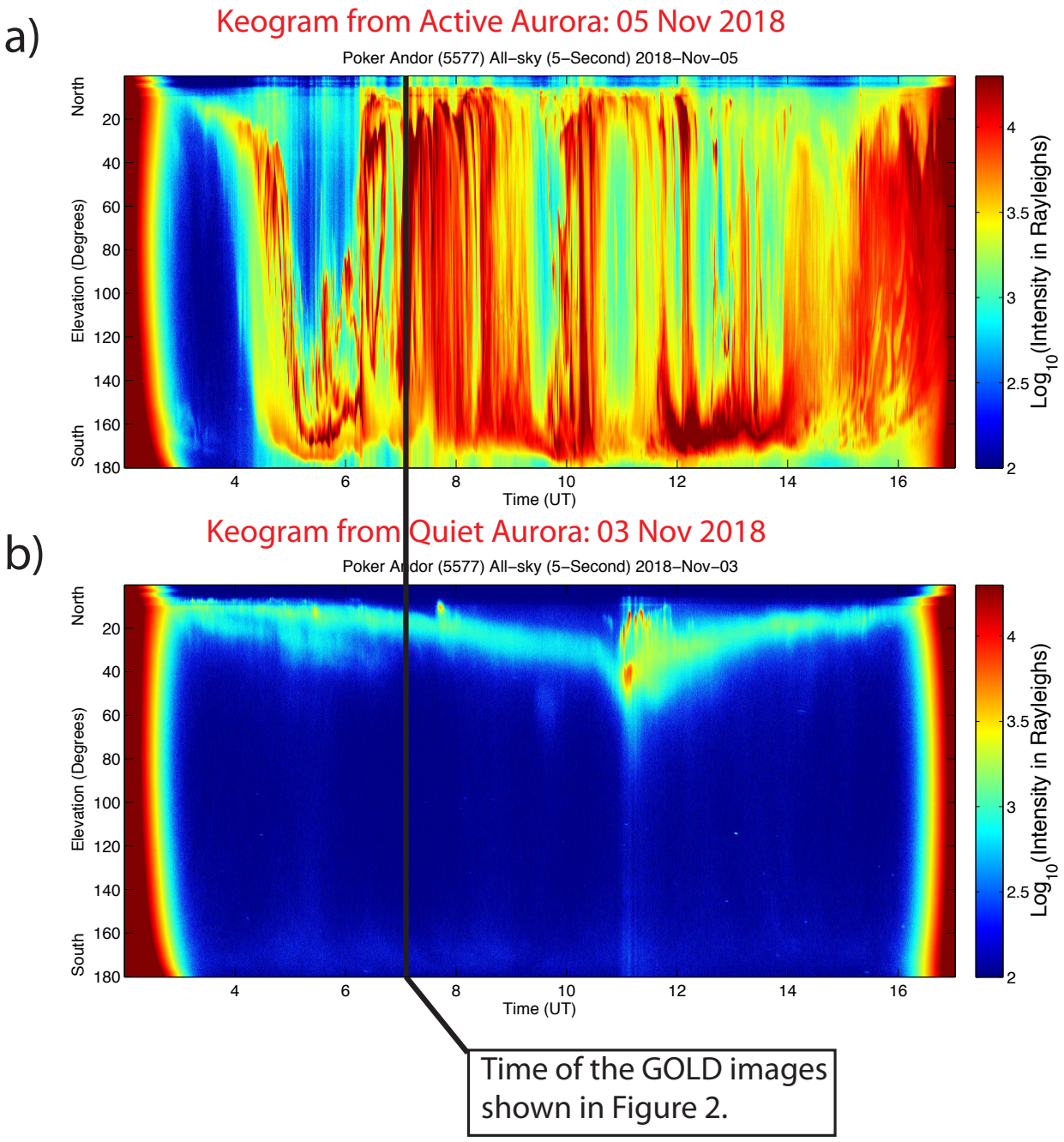

Figure 3. Keograms of 557.7 nm visible-light aurora from Poker Flat, AK for the same two nights as the GOLD data presented in Figure 2 and displayed on the same intensity scale. The black vertical line represents the time when the GOLD images were taken.

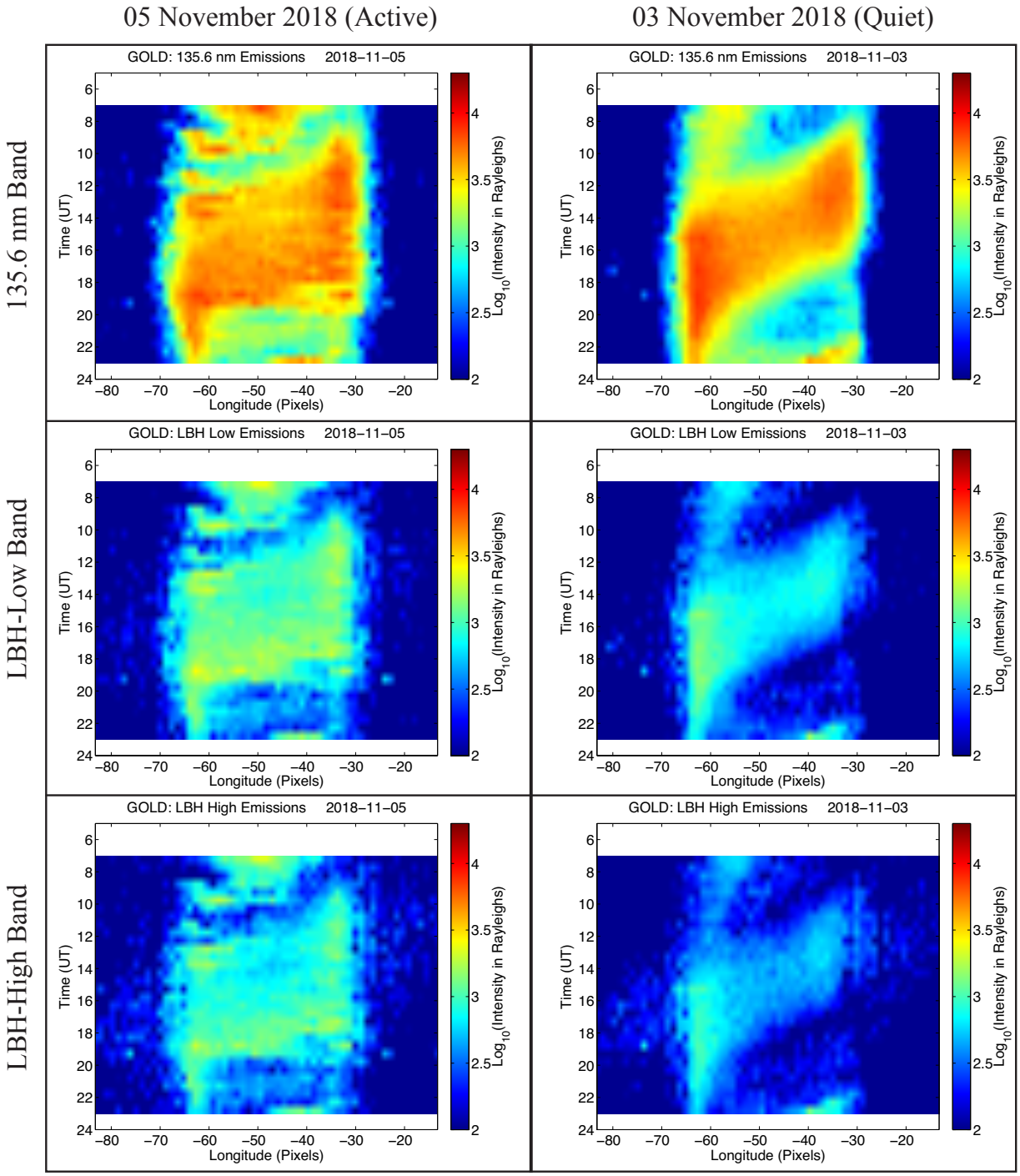

Figure 4. East-west keograms constructed from the GOLD images for 05 Nov 2018 (active aurora) and 03 Nov 2018 (quiet aurora) for the three wavelength bands of interest. All three wavelength bands are plotted on the same intensity scale for accurate comparison.

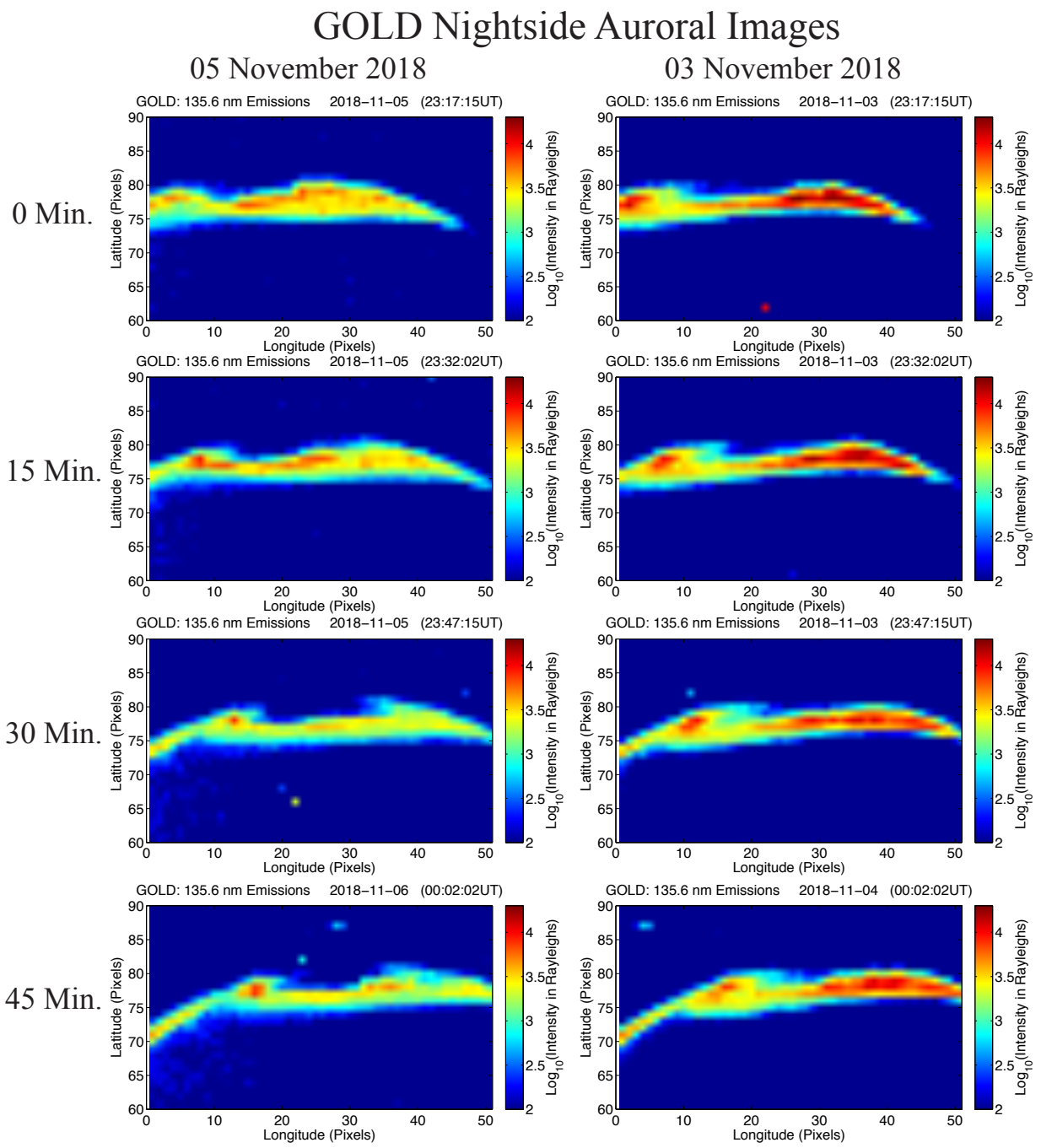

Figure 5. Time-series of GOLD nightside images of the aurora (in the 135.6 nm band) for two different nights. 05 November, which was the active auroral night (left column) and 03 November, which was the quiet auroral night (right column). These images are spaced 15 minutes apart, covering 45 minutes with the four images.

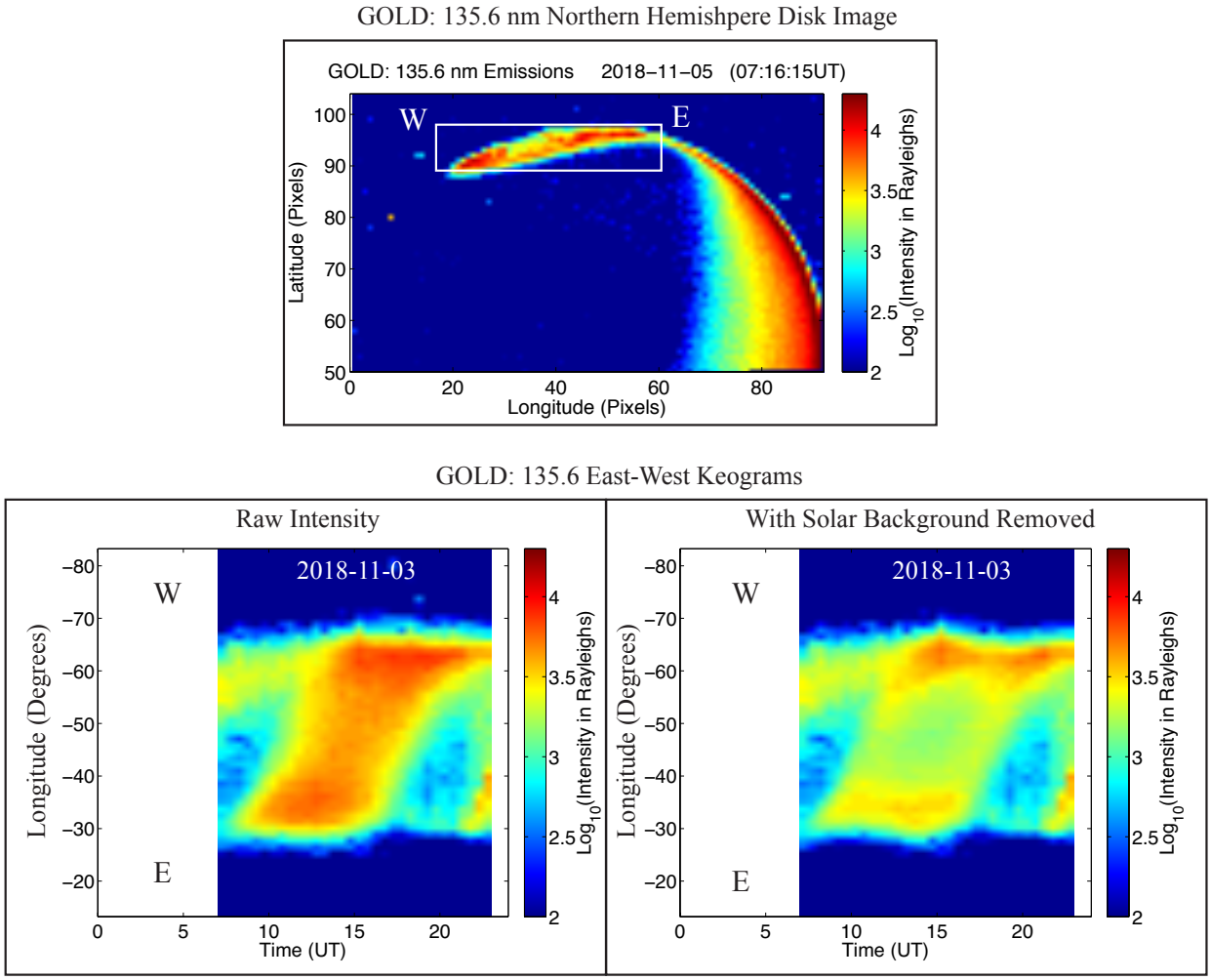

Figure 6. GOLD disk image with the auroral region of interest highlighted by a white box (top). Comparison between a keogram created from the raw intensity (left) and one created from the intensity with the solar contamination removed by subtracting off the simple model of the solar induced background (right).

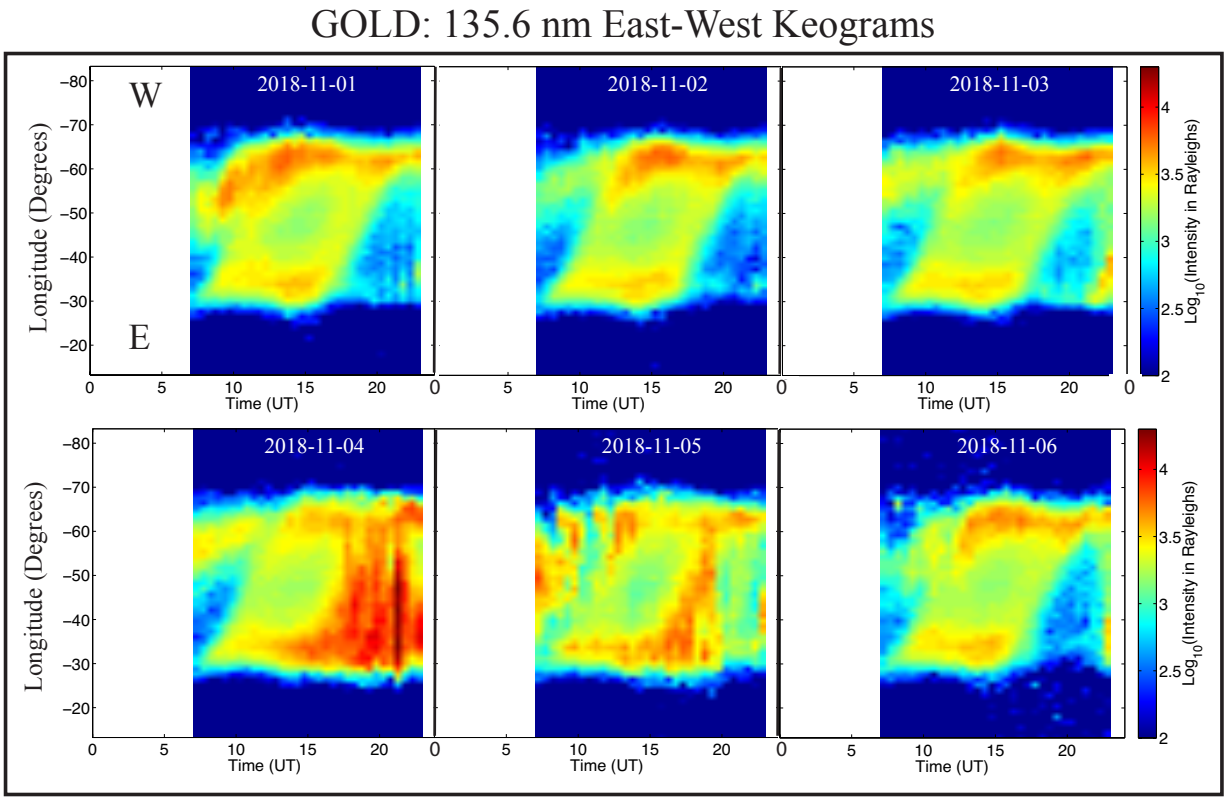

Figure 7. Consecutive time-series of longitudinal keograms constructed from the 135.6 nm band dayside GOLD images of the aurora for six days (01–06 November 2018).